

Anderson Transition for Classical Transport in Composite Materials

N. Benjamin Murphy, Elena Cherkaev, and Kenneth M. Golden*

Department of Mathematics, University of Utah, 155 S 1400 E RM 233, Salt Lake City, Utah 84112-0090, USA

(Received 4 May 2016; revised manuscript received 27 October 2016; published 19 January 2017)

The Anderson transition in solids and optics is a wave phenomenon where disorder induces localization of the wave functions. We find here that the hallmarks of the Anderson transition are exhibited by classical transport at a percolation threshold—without wave interference or scattering effects. As long range order or connectedness develops, the eigenvalue statistics of a key random matrix governing transport cross over toward universal statistics of the Gaussian orthogonal ensemble, and the field eigenvectors delocalize. The transition is examined in resistor networks, human bone, and sea ice structures.

DOI: [10.1103/PhysRevLett.118.036401](https://doi.org/10.1103/PhysRevLett.118.036401)

Introduction.—The Anderson theory of the metal-insulator transition (MIT) [1,2] provides a powerful, quantum mechanical framework for understanding when a disordered medium allows electronic transport, and when it does not. Indeed, for large enough disorder the electrons are localized in different places, with uncorrelated energy levels described by Poisson statistics [3,4]. For small disorder, the wave functions are extended and overlap, giving rise to correlated Wigner-Dyson (WD) energy level statistics [3,4] with strong level repulsion [5]. For intermediate disorder hybrid Poisson-like level statistics arise [3,4,6,7].

Here, we consider the effective transport coefficients of macroscopic two phase composites in 2D and 3D [8–10], including electrical and thermal conductivity, diffusivity, complex permittivity, and magnetic permeability. All are formulated with the same elliptic partial differential equation. For example, electrical conduction is described by $\nabla \cdot (\sigma \nabla \phi) = 0$ with potential ϕ , electric field $\mathbf{E} = -\nabla \phi$, and local conductivity σ taking the values σ_1 or σ_2 . A metal-insulator mixture is modeled with $h = \sigma_1/\sigma_2 \rightarrow 0$. Near a percolation threshold the system undergoes a classical MIT with the effective conductivity σ^* described by critical exponents [10–12].

The underlying physics of the quantum and classical MIT are quite different. Anderson localization in quantum systems, described by the Schrödinger equation, is a wave interference phenomenon, and should be universal to all wave systems, such as in optics where it has been investigated extensively [13]. On the other hand, for transport in macroscopic two phase media governed by the elliptic equation above, there are no wave interference or scattering effects and no quantum phenomena.

It is surprising then that the self-adjoint random operator G governing effective transport in composites has spectral properties that transition in a way that is strikingly similar to the Anderson transition in wave mechanics. We find here that phase connectedness in composites determines the Anderson-like transition in the spectral properties of G . The critical volume fraction at the percolation threshold [11]

plays the role of the critical level of disorder necessary for localization in wave physics.

The operator G arises in the analytic continuation method [14–16] for studying transport in two phase composites. Stieltjes integral representations for the bulk transport coefficients such as σ^* incorporate the two phase mixture geometry in a spectral measure μ of G [16]. For discrete media such as the random resistor network (RRN) [11], G is a real-symmetric random matrix and the spectral measure μ as well as the electric field \mathbf{E} are given explicitly in terms of its eigenvalues and eigenvectors [10,17]. The locations of the eigenvalues along the negative real axis in the h plane correspond to singularities of the bulk transport coefficients [8,10,12,18].

We observe that as the conducting phase percolates, the eigenvectors of G shift from localized to extended, causing the electric field \mathbf{E} to spread throughout the system. Near the connectedness-driven MIT mobility edges appear, analogous to Anderson localization where mobility edges mark the characteristic energies of the quantum MIT [5]. The overlap of eigenvectors of G gives rise to a transition in the statistical properties of the eigenvalues from weakly correlated Poisson-like statistics toward universal WD statistics of the Gaussian orthogonal ensemble (GOE) with strong level repulsion [3–5]. This eigenvalue repulsion explains the collapse of spectral gaps as connectedness develops [17–20], which is closely related to critical behavior [10,12,18–22].

To help connect our findings to the physics of disordered media, we consider two systems whose optical properties are determined by the spectral characteristics considered here, and where our findings may have observable consequences: metallic particles in an insulating host, such as colloidal suspensions of gold nanoparticles in a liquid [10], and metal films such as depositions of nanosized metal particles on a dielectric substrate [23]. The long wavelength quasistatic assumption holds in the visible range, and these systems are described macroscopically by an effective complex permittivity ϵ^* , and locally by the above elliptic

partial differential equation with local complex permittivity values $\epsilon_1(\omega)$ and $\epsilon_2(\omega)$. Values of $h = \epsilon_1/\epsilon_2$ near the negative real axis can be realized in these systems over certain ranges of frequency ω [10]. The resonance structure of ϵ^* and the absorption profile, such as sharp peaks associated with surface plasmon resonances [10,23], are then observable [10,12] and determined by the spectral properties of G . For finite discrete models [10,12,18,23], such as binary RL - C networks where metallic bonds consist of a resistor in series with an inductor and dielectric bonds consist of a capacitor [12,18], the eigenvalues of the matrix G are poles of the effective complex conductivity, which collectively give rise to network resonances. Indeed, geometrical disorder in these media leads to a broad range of surface plasmon resonances analogous to RL - C resonances, and strong enhancement of the local electric fields [23]. Our findings on the transition to universality of the resonance spacing distribution, for example, may be observable through analysis of the fine structure of the absorption spectra. Interestingly, WD universality has been observed in microwave absorption spectra of a suspension of metal particles at low temperature, where the energy level spacing distribution for electronic states in the grains determines the conductivity [24].

As remarked above, the physics of the quantum and classical MIT are different. Thus, we emphasize that the similarities to the Anderson transition described here are mathematical in nature and one cannot expect a similarity in all physical aspects. For example, the dependence of the conductivity on the eigenvalues and eigenvectors is different in the quantum and classical cases. Moreover, in quantum conduction a magnetic field breaks time reversibility, yielding a Hermitian random matrix and a crossover to universal WD statistics of the Gaussian unitary ensemble, instead of the GOE associated with time reversibility and a real-symmetric random matrix [25]. The Anderson transition to Gaussian unitary ensemble universality has been captured by an exactly solvable model [4,7], while the transition to GOE universality remains open.

In random matrix theory [5,26,27], long and short range correlations of the eigenvalues [5,6] of matrices with random entries are measured using various statistics [5,26], such as the eigenvalue spacing distribution (ESD). Eigenvector localization is often described by the inverse participation ratio (IPR) [2,28]. A fascinating feature of random matrix theory is that eigenvalue statistics arising in a broad range of unrelated systems exhibit the same universal behavior—from nuclear spectra [5,26] and mesoscopic conductors [25] to random graphs [29] and quantum chaos [5]. Here, we explore the transition to GOE universality in the 2D and 3D RRN, as well as in 2D discretizations of the brine microstructure of sea ice [30,31], melt ponds on the surface of Arctic sea ice [32], the sea ice pack itself, and porous human bone [33].

Mathematical methods.—Consider conduction in two phase composites [8,10,16,17], where \mathbf{E} and \mathbf{J} are the electric

and current density fields satisfying $\mathbf{J} = \sigma\mathbf{E}$, $\nabla \cdot \mathbf{J} = 0$, and $\nabla \times \mathbf{E} = 0$, and σ is the local conductivity. For a stationary random medium in 2D or 3D with component conductivities σ_1 and σ_2 , $\sigma = \sigma_1\chi_1 + \sigma_2\chi_2$, where $\chi_1 = 1$ in medium 1 and is zero otherwise, with $\chi_2 = 1 - \chi_1$.

The effective conductivity matrix σ^* can be defined by $\langle \mathbf{J} \rangle = \sigma^* \langle \mathbf{E} \rangle$ with average field $\langle \mathbf{E} \rangle = \mathbf{E}_0$. Here, $\langle \cdot \rangle$ denotes ensemble averaging over the probability distribution defining the random medium, and $\mathbf{E}_0 = E_0\mathbf{e}_1$, for example, where \mathbf{e}_1 is a unit vector in the x direction [16]. Equivalently, we find ϕ satisfying $\nabla \cdot (\sigma\nabla\phi) = 0$ in the 2D square $[-L, L] \times [-L, L]$, or 3D cube, $\phi(-L, y) = -LE_0$, and $\phi(L, y) = LE_0$ for $-L \leq y \leq L$, and $\partial\phi/\partial y = 0$ on the top and bottom, so that $\langle \mathbf{E} \rangle_L = \mathbf{E}_0$. Here $\langle \cdot \rangle_L$ is spatial average. The effective conductivity matrix σ_L^* is defined by $\langle \mathbf{J} \rangle_L = \sigma_L^* \langle \mathbf{E} \rangle_L$. For stationary, ergodic σ , $\lim_{L \rightarrow \infty} \sigma_L^* = \sigma^*$ (see the appendix in Ref. [16]).

The key to the analytic continuation method is the Stieltjes integral representation [14–17]

$$F(s) = 1 - \frac{\sigma^*}{\sigma_2} = \int_0^1 \frac{d\mu(\lambda)}{s - \lambda}, \quad s = \frac{1}{1 - \sigma_1/\sigma_2}, \quad (1)$$

where we focus on a diagonal coefficient $\sigma^* = \sigma_{kk}^*$ of the matrix σ^* for isotropic media. Equation (1) follows from the resolvent formula for the electric field [16,17]

$$\chi_1 \mathbf{E} = s(sI - G)^{-1} \chi_1 \mathbf{E}_0, \quad (2)$$

and $F(s) = \langle \chi_1 \mathbf{E} \cdot \mathbf{E}_0 \rangle / (sE_0^2)$, where μ is a spectral measure of the random operator $G = \chi_1 \Gamma \chi_1$ and $\Gamma = -\nabla(-\Delta)^{-1}\nabla$ is the projection onto curl-free fields, based on convolution with the Green's function for the Laplacian $\Delta = \nabla^2$. Parameter information in s is separated from mixture geometry information, which is encoded into μ via its moments, $\mu_n = \int_0^1 \lambda^n d\mu(\lambda)$. For example, $\mu_0 = \langle \chi_1 \rangle = p$, the volume fraction of medium 1. All of the effective properties of the composite are represented via Stieltjes integrals with the same μ [34]. The measure μ reduces to a weighted sum of Dirac δ -functions $\delta(\lambda - \lambda_j)$ for media such as laminates, hierarchical coated cylinder and sphere assemblages, and finite resistor networks [8].

Consider a square $d = 2$ RRN in $[0, L] \times [0, L]$, with conducting bars along $x = 0$ and $x = L$ and periodic boundary conditions at $y = 0$ and $y = L$, and its cubic $d = 3$ analog. In this case, $G = \chi_1 \Gamma \chi_1$ is a real-symmetric random matrix of size $N = L^d d$ [17], χ_1 is a diagonal matrix with 1's and 0's along the diagonal corresponding to bond type, and Γ is a projection matrix [17]. The measure μ is determined by the eigenvalues λ_j and eigenvectors \mathbf{v}_j of $N_1 \times N_1$ submatrices of Γ corresponding to diagonal components $[\chi_1]_{jj} = 1$, $d\mu = \sum_j \langle m_j \delta(\lambda - \lambda_j) \rangle d\lambda$, where $m_j = [\mathbf{v}_j \cdot \chi_1 \mathbf{e}_k]^2$, $j = 1, \dots, N_1$, $N_1 \approx pN$ [17].

To calculate eigenvalue and eigenvector statistics, we have converted 2D images of sea ice and bone to resistor

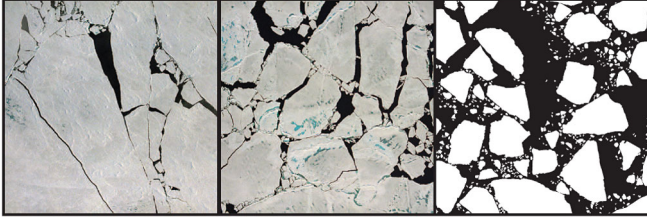


FIG. 1. Connectedness transition in composite structures. Images of the Arctic sea ice pack (photo credit D. K. Perovich) with increasingly connected ocean phase from left to right.

networks. Figure 1 displays images of the Arctic ice pack with a binary version on the far right. The matrix $G = \chi_1 \Gamma \chi_1$ is then obtained for these binary discretizations.

Finally, consider the time dependent Schrödinger equation $i\hbar \partial \psi / \partial t = H \psi$, and the Laplace transform $\Psi(\mathbf{x}, s)$ of $\psi(\mathbf{x}, t)$, as in Ref. [1] (here s is the transform variable). Then, $\Psi(\mathbf{x}, s)$ has a resolvent representation analogous to Eq. (2), $\Psi(\mathbf{x}, s) = (i\hbar s I - H)^{-1} \psi(\mathbf{x}, 0)$. Then, G for classical transport is an analog of the Hamiltonian H .

Numerical results.—For highly correlated WD spectra of the GOE, the nearest neighbor ESD $P(z)$ is accurately approximated by $P(z) \approx (\pi z/2) \exp(-\pi z^2/2)$, which illustrates eigenvalue repulsion, vanishing linearly as spacings $z \rightarrow 0$ [5,6,25]. In contrast, the ESD for uncorrelated Poisson spectra, $P(z) = \exp(-z)$, allows for level degeneracy [5].

In Fig. 2 we display the ESDs for Poisson and GOE spectra, along with the ESDs for G corresponding to sea ice composite structures with fluid area fraction p and the 2D RRN with a fraction p of phase 1. [To observe statistical fluctuations of eigenvalues about the mean density $\rho(\lambda)$ [5,26], the spectrum must be unfolded [5,6,28].] It shows

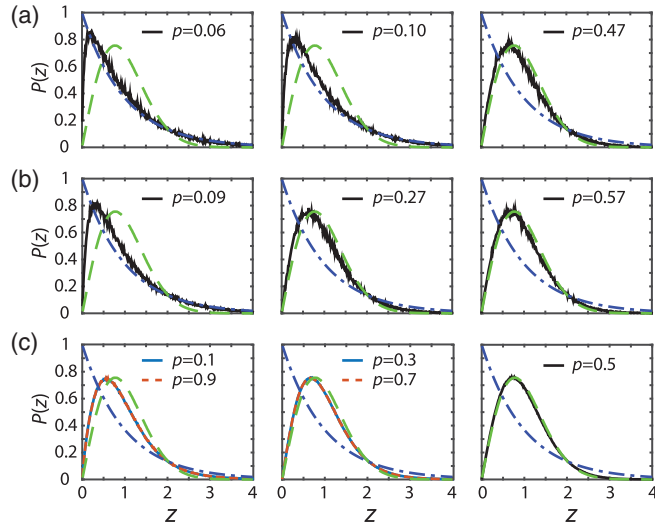


FIG. 2. Short-range eigenvalue correlations. The ESDs for Poisson (blue dash dot) and WD (green dashed) spectra are shown in (a)–(c), along with ESDs for (a) the Arctic sea ice pack, (b) Arctic melt ponds, and (c) the 2D RRN.

that for sparsely connected systems, the behavior of the ESDs is well described by weakly correlated Poisson-like statistics [6]. They increase linearly from zero but the initial slope of the curve is steeper than in the WD case, implying less repulsion, and the tails decay exponentially. With increasing connectedness, the ESDs transition toward highly correlated WD statistics with strong level repulsion and Gaussian tails. For the 2D and 3D RRN, the eigenvalue density $\rho(\lambda, p)$ obeys $\rho(\lambda, p) = \rho(1 - \lambda, 1 - p)$ in the bulk of the spectrum. This is reflected in the ESDs by the symmetry $P(z, p) = P(z, 1 - p)$, as shown for the 2D RRN in Fig. 2(c).

Long-range eigenvalue correlations are measured by quantities such as the eigenvalue number variance $\Sigma^2(L)$, in intervals of length L (not to be confused with the system size L), and the spectral rigidity $\Delta_3(L)$ [5]. For uncorrelated Poisson spectra, these long range statistics are linear, with $\Sigma^2(L) = L$ and $\Delta_3(L) = L/15$. In contrast, the strong correlations of WD spectra make the spectrum more rigid [6] so that $\Sigma^2(L)$ and $\Delta_3(L)$ grow only logarithmically [5].

In Fig. 3 we display $\Sigma^2(L)$ and $\Delta_3(L)$ for Poisson and WD spectra [5], along with those for the matrix G for macroscopic composite structures. For sparsely connected systems, these statistics exhibit linear Poisson-like behavior away from the origin with slope less than their Poisson counterparts. This linear behavior has been attributed to exponentially decaying correlations of eigenvalues [6]. With increasing connectedness, these statistics transition toward logarithmic WD behavior typical of the GOE, which has quadratically decaying eigenvalue correlations [6]. Similar to the ESDs in Fig. 2, for the RRN these statistics also display the symmetry $\Sigma^2(L, p) = \Sigma^2(L, 1 - p)$ and $\Delta_3(L, p) = \Delta_3(L, 1 - p)$.

Moreover, Fig. 3(f) suggests that the GOE limit is attained by the long range statistics for the 3D RRN for all $p_c \leq p \leq 1 - p_c$. The computed ESDs also appear to

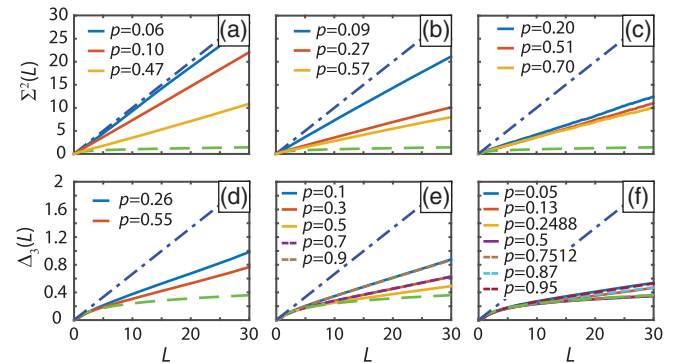


FIG. 3. Long-range eigenvalue correlations. (a)–(c) The eigenvalue number variance $\Sigma^2(L)$ and (d)–(f) the spectral rigidity $\Delta_3(L)$ for Poisson (blue dash dot) and WD (green dashed) spectra are shown along with those of (a) Arctic pack ice, (b) Arctic melt ponds, (c) sea ice brine inclusions, (d) human bone microstructure, (e) the 2D RRN, and (f) the 3D RRN.

overlie the GOE limit almost exactly for all p values tested in $p_c \leq p \leq 1 - p_c$. With this in mind, we recall the Anderson transition, where low disorder corresponds to extended states and WD statistics. When disorder exceeds a critical level, the states localize and the eigenvalues become decorrelated. We view the 3D RRN with $p_c \leq p \leq 1 - p_c$ to be “ordered” with extended states and WD statistics. As p decreases, the disorder—or blockages to the flow—increases, and the eigenstates localize.

The eigenvectors \mathbf{v}_j associated with the random $N_1 \times N_1$ submatrices of Γ exhibit a connectedness driven transition in their localization properties. The IPR I_j [28] is defined as $I_j = \sum_i [v_j^i]^4$, $i, j = 1, \dots, N_1$, where v_j^i is the i th component of \mathbf{v}_j . Two limiting cases illustrate the meaning of I_j : (i) a normalized vector with only one component $v_j^i = 1$ has $I_j = 1$; (ii) a vector with identical components $v_j^i = 1/\sqrt{N_1}$ has $I_j = 1/N_1$. Eigenvectors of matrices in the GOE are known to be highly extended and independent of the distribution of the eigenvalues [27], and the IPR is given by $I_{\text{GOE}} = 3/N_1$ [28].

In the matrix setting, the electric field in Eq. (2) has the following eigenvector expansion

$$\chi_1 \mathbf{E} = sE_0 \sum_j [(s - \lambda_j)^{-1} (\mathbf{v}_j \cdot \chi_1 \mathbf{e}_k)] \mathbf{v}_j. \quad (3)$$

This provides a direct link between localized eigenvectors \mathbf{v}_j and eigenmodes of $\chi_1 \mathbf{E}$ with large magnitudes in only a few resistors, while extended eigenvectors correspond to fields extending throughout the network. Figure 4(a) shows the electric field $\chi_1 \mathbf{E}$ for the 2D RRN with $p = p_c = 1/2$.

We have plotted the IPR I_j for the 2D and 3D RRN, as functions of λ_j and j , with increasing j corresponding to increasing magnitude of λ_j . Our results have revealed that the eigenvectors \mathbf{v}_j delocalize as p increases and the system becomes increasingly connected. Specifically, for $p \ll p_c$, the eigenvectors are localized, with values of I_j much larger than the GOE IPR. Also, I_j is oscillatory as a function of λ_j ,

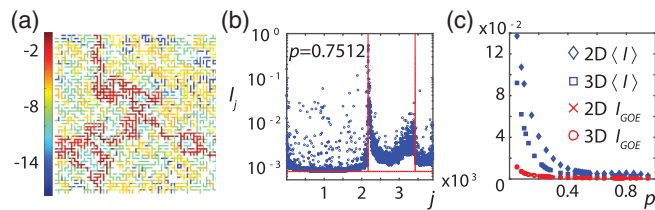


FIG. 4. Delocalization of eigenvectors. (a) The electric field $\chi_1 \mathbf{E}$ (in log scale) for a realization of the 2D RRN, with a system size $L = 50$, volume fraction $p = p_c = 1/2$, and $\sigma_1/\sigma_2 = 4.0 \times 10^{10}$. (b) The IPR I_j plotted versus the index $j = 1, \dots, N_1$ for a realization of the 3D RRN with $L = 12$ and $p = 1 - p_c \approx 0.7512$. The vertical lines define the δ components of the spectral measure μ at $\lambda = 0, 1$, while the horizontal line marks the GOE IPR value $I_{\text{GOE}} = 3/N_1$. (c) The p dependence of the average IPR $\langle I \rangle$ for the 2D and 3D RRN.

following the peaks and valleys of “geometric” resonances exhibited by $\rho(\lambda)$ for small p [17,18], with localized regions corresponding to lower density. This indicates significant correlation between the eigenvalues and eigenvectors, contrasting the GOE.

As $p \rightarrow p_c^-$, spectral gaps around the end points shrink and vanish [17,18], while the I_j continually decrease. As p surpasses p_c and $1 - p_c$, δ components form in μ at $\lambda = 0$ and $\lambda = 1$, respectively [19]. The δ component at $\lambda = 0$ is manifested by a large number of λ_j with magnitude $\lesssim 10^{-14}$, followed by an abrupt change of magnitude $\gtrsim 10^{-4}$, with no eigenvalues in the interval $(10^{-14}, 10^{-4})$, and similarly for $\lambda = 1$. Figure 4(b) displays I_j for the 3D RRN with $p = 1 - p_c \approx 0.7512$, plotted versus index j . The locations of the abrupt changes in eigenvalue magnitudes are identified by red vertical lines, while the GOE IPR value is identified by the red horizontal line. This figure demonstrates that eigenvectors associated with the δ components at $\lambda = 0, 1$ are typically more extended than others, with I_j values closer to the GOE limit.

This delocalization of the eigenvectors can be seen in Fig. 4(c), which displays the p dependence of $\langle I \rangle$ over all values of I_j . As p and system connectedness increase, $\langle I \rangle$ decreases, with transitional behavior at p_c . This indicates that the eigenvectors (and eigenmodes of \mathbf{E}) become progressively extended throughout the network. Figure 4(b) indicates that this average delocalization is largely due to the formation of the δ components in μ at $\lambda = 0, 1$.

Figure 4(b) also shows that regions of extended states are separated by “mobility edges” with a sudden increase in the number of localized eigenvectors, which is analogous to Anderson localization, where mobility edges mark the characteristic energies of the MIT [5]. Interestingly, the mobility edges in Fig. 4(b) are found at the locations of the δ components (red vertical lines), which control critical behavior of transport in insulator-conductor and conductor-superconductor systems [10,12,19].

Conclusions.—We have demonstrated that the statistical behavior of the eigenvalues and eigenvectors of the random matrix $G = \chi_1 \Gamma \chi_1$ governing classical transport through composites—in the absence of wave interference and quantum effects—undergoes a percolation-driven transition that is analogous to the Anderson transition in wave physics. The eigenvalues—or resonances in the bulk transport coefficients—shift from weakly correlated Poisson-like statistics toward highly correlated universal WD statistics of the GOE, as a function of order or connectedness. Correspondingly, the eigenvectors undergo a delocalization, with highly extended states appearing at the spectral end points, separated by mobility edges of localized states. The delocalization of eigenvectors corresponds to an extended transport field, such as the electric field \mathbf{E} , extending throughout the composite near global connectedness thresholds. The percolation-driven transition to repulsive eigenvalue behavior also accounts for the vanishing

gaps in the support of the spectral measure μ , which is closely connected to critical behavior of transport. Our results open the door to applying ideas and methods from Anderson localization to classical transport, and open a new chapter in the application of random matrix theory to complex macroscopic systems.

We gratefully acknowledge support from the Division of Mathematical Sciences and the Division of Polar Programs at the U.S. National Science Foundation (NSF) through Grants No. DMS-1009704, No. ARC-0934721, No. DMS-0940249, and No. DMS-1413454. We are also grateful for support from the Office of Naval Research (ONR) through Grants No. N00014-13-10291 and No. N00014-12-10861. Finally, we would like to thank Mikhail Raikh, Gérard Ben Arous, and the anonymous referees for very helpful comments on our work and the Letter, and the Math Climate Research Network (MCRN) for their support.

*golden@math.utah.edu

- [1] P. Anderson, Absence of diffusion in certain random lattices, *Phys. Rev.* **109**, 1492 (1958).
- [2] F. Evers and A. D. Mirlin, Anderson transitions, *Rev. Mod. Phys.* **80**, 1355 (2008).
- [3] B. I. Shklovskii, B. Shapiro, B. R. Sears, P. Lambrianides, and H. B. Shore, Statistics of spectra of disordered systems near the metal-insulator transition, *Phys. Rev. B* **47**, 11487 (1993).
- [4] V. E. Kravtsov and K. A. Muttalib, New Class of Random Matrix Ensembles with Multifractal Eigenvectors, *Phys. Rev. Lett.* **79**, 1913 (1997).
- [5] T. Guhr, A. Müller-Groeling, and H. A. Weidenmüller, Random-matrix theories in quantum physics: Common concepts, *Phys. Rep.* **299**, 189 (1998).
- [6] C. M. Canali, Model for a random-matrix description of the energy-level statistics of disordered systems at the Anderson transition, *Phys. Rev. B* **53**, 3713 (1996).
- [7] K. A. Muttalib, Y. Chen, M. E. H. Ismail, and V. N. Nicopoulos, New Family of Unitary Random Matrices, *Phys. Rev. Lett.* **71**, 471 (1993).
- [8] G. W. Milton, *Theory of Composites* (Cambridge University Press, Cambridge, England, 2002).
- [9] S. Torquato, *Random Heterogeneous Materials: Microstructure and Macroscopic Properties* (Springer-Verlag, New York, 2002).
- [10] D. J. Bergman and D. Stroud, Physical properties of macroscopically inhomogeneous media, *Solid State Phys.* **46**, 147 (1992).
- [11] D. Stauffer and A. Aharony, *Introduction to Percolation Theory*, 2nd ed. (Taylor and Francis, London 1992).
- [12] J. P. Clerc, G. Giraud, J. M. Laugier, and J. M. Luck, The electrical conductivity of binary disordered systems, percolation clusters, fractals, and related models, *Adv. Phys.* **39**, 191 (1990).
- [13] M. Segev, Y. Silberberg, and D. N. Christodoulides, Anderson localization of light, *Nat. Photonics* **7**, 197 (2013).
- [14] D. J. Bergman, Exactly Solvable Microscopic Geometries and Rigorous Bounds for the Complex Dielectric Constant of a Two-Component Composite Material, *Phys. Rev. Lett.* **44**, 1285 (1980).
- [15] G. W. Milton, Bounds on the complex dielectric constant of a composite material, *Appl. Phys. Lett.* **37**, 300 (1980).
- [16] K. Golden and G. Papanicolaou, Bounds for effective parameters of heterogeneous media by analytic continuation, *Commun. Math. Phys.* **90**, 473 (1983).
- [17] N. B. Murphy, E. Cherkaev, C. Hohenegger, and K. M. Golden, Spectral measure computations for composite materials, *Commun. Math. Sci.* **13**, 825 (2015).
- [18] T. Jonckheere and J. M. Luck, Dielectric resonances of binary random networks, *J. Phys. A* **31**, 3687 (1998).
- [19] N. B. Murphy and K. M. Golden, The Ising model and critical behavior of transport in binary composite media, *J. Math. Phys. (N.Y.)* **53**, 063506 (2012).
- [20] A. R. Day and M. F. Thorpe, The spectral function of random resistor networks, *J. Phys. Condens. Matter* **8**, 4389 (1996).
- [21] G. A. Baker, *Quantitative Theory of Critical Phenomena* (Academic Press, New York, 1990).
- [22] K. M. Golden, Critical Behavior of Transport in Lattice and Continuum Percolation Models, *Phys. Rev. Lett.* **78**, 3935 (1997).
- [23] D. A. Genov, V. M. Shalaev, and A. K. Sarychev, Surface plasmon excitation and correlation-induced localization-delocalization transition in semicontinuous metal films, *Phys. Rev. B* **72**, 113102 (2005).
- [24] F. Zhou, B. Spivak, N. Taniguchi, and B. L. Altshuler, Giant Microwave Absorption in Metallic Grains: Relaxation Mechanism, *Phys. Rev. Lett.* **77**, 1958 (1996).
- [25] A. D. Stone, P. A. Mello, K. A. Muttalib, and J. L. Pichard, Random matrix theory and maximum entropy models for disordered conductors, in *Mesoscopic Phenomena in Solids* (Elsevier, Amsterdam, 1991), Chap. 9, pp. 369–448.
- [26] O. Bohigas and M.-J. Giannoni, Chaotic motion and random matrix theories, in *Mathematical and Computational Methods in Nuclear Physics*, Lecture Notes in Physics Vol. 209 (Springer, Berlin, 1984), pp. 1–99.
- [27] P. Deift and D. Gioev, *Random Matrix Theory: Invariant Ensembles and Universality* (American Mathematical Society, Courant Institute of Mathematical Sciences, New York, 2009).
- [28] V. Plerou, P. Gopikrishnan, B. Rosenow, L. A. N. Amaral, T. Guhr, and H. E. Stanley, Random matrix approach to cross correlations in financial data, *Phys. Rev. E* **65**, 066126 (2002).
- [29] J. N. Bandyopadhyay and S. Jalan, Universality in complex networks: Random matrix analysis, *Phys. Rev. E* **76**, 026109 (2007).
- [30] K. M. Golden, S. F. Ackley, and V. I. Lytle, The percolation phase transition in sea ice, *Science* **282**, 2238 (1998).
- [31] K. M. Golden, H. Eicken, A. L. Heaton, J. Miner, D. Pringle, and J. Zhu, Thermal evolution of permeability and microstructure in sea ice, *Geophys. Res. Lett.* **34**, L16501 (2007).
- [32] C. Hohenegger, B. Alali, K. R. Steffen, D. K. Perovich, and K. M. Golden, Transition in the fractal geometry of Arctic melt ponds, *The Cryosphere* **6**, 1157 (2012).
- [33] K. M. Golden, N. B. Murphy, and E. Cherkaev, Spectral analysis and connectivity of porous microstructures in bone, *J. Biomech.* **44**, 337 (2011).
- [34] E. Cherkaev, Inverse homogenization for evaluation of effective properties of a mixture, *Inverse Probl.* **17**, 1203 (2001).